JOURNAL OF MATERIALS SCIENCE **36** (2001) 461–468

The sequence of precipitation in 339 aluminum castings

R. K. MISHRA, G. W. SMITH, W. J. BAXTER, A. K. SACHDEV, V. FRANETOVIC
General Motors Research and Development Center, Warren, Michigan, USA

The precipitation sequences in direct-quenched from the die (DQD) and solution-treated (SOL) 339 aluminum have been determined by a combination of differential scanning calorimetry (DSC) and transmission electron microscopy (TEM). DSC scans for the alloy in both conditions exhibit two distinct exothermic peaks, each associated with a unique precipitate. The peak temperatures for precipitation in the DQD and SOL alloys differ by only a few degrees. TEM of samples heated to the lower temperature peak shows that the first precipitate to form in the DQD alloy is S' (Al_2CuMg), whereas in the SOL alloy it is β' (Mg_2Si). The principal precipitate associated with the higher temperature peak in both DQD and SOL alloys is Si. The DSC peak temperature identifies the specific precipitate in 339 Al, but the peak area is not a reliable measure of precipitate density. Nano-indentation of the dendrites shows that the strength provided by the precipitates increases in the sequence $Si < S' < \beta'$. However, their thermal stability increases in the reverse order.

1. Introduction

It is well known that the formation of precipitates in the aluminum lattice plays a dominant role in determining the strength of many aluminum alloys. Indeed, this factor alone has dictated the development of many commercial alloys, which encompass a wide range of alloying elements—and consequently precipitate compositions. This variety is compounded further by a selection of heat treatments, which for many alloys substantially affects the mechanical properties by virtue of changes in the nature and/or distribution of the precipitates. Thus, an essential key to understanding lies in characterizing the precipitates—namely their composition, structure, and crystallographic relationship to the host aluminum lattice (i.e., the parameters controlling their effectiveness in impeding dislocation motion). In this regard, the only unequivocal evidence is provided by transmission electron microscopy (TEM), in combination with microanalysis by X-ray emission or electron energy loss spectroscopy. However, these sophisticated techniques are very time consuming and not suitable for routine analysis. Furthermore, only an extremely small volume of material can be examined, which may not always be representative of the overall condition of the alloy.

A much simpler and more rapid measure of the precipitation process is provided by differential scanning calorimetry (DSC). This technique uses a larger specimen (~100 mg) and so provides a more representative macroscopic view. Calorimetry has been applied to investigations of a range of aluminum alloys [1–32]. In a DSC experiment the rate of heat evolution (or absorption) is plotted as a function of temperature, and a precipitation event is manifested as an exothermic peak. For a given heating rate, the peak temperature depends upon the specific precipitate and/or the rate-controlling diffusion process. In fact, precipitation kinetics can be determined by an analysis due to Kissinger and others [33–39] which relates the peak temperature to the temperature scan rate.

However, a major difficulty is to identify the precipitate responsible for a particular exothermic peak. In this regard, a survey of the literature reveals a consensus that, at heating rates near 20 °C/min, peaks in the range of 70 to 150 °C are associated with the formation of various GP zones [4, 6–8, 11–15, 17, 19–29, 32]. But for precipitation peaks in the range 200 to 350 °C there have been disagreements: as Oguocha and Yannacopoulos [28] point out, the literature is not definitive regarding precipitation peak temperatures because of such factors as previous thermal history, material, and DSC heating rate. Examples include differences due to fabrication methods in alloys 2219 and 6061 [6], silicon concentration in AlMgSi alloys [29], and precipitate identification in solutionized alloys 6061 [11, 13–15, 19, 20, 24] and 2124 [6, 25, 32]. Peak temperature inconsistencies could arise in two ways: (i) if nucleation is not homogeneous but is catalyzed by some extraneous agency, and (ii) if the assignments are not based upon the rigors of TEM correlations. Clearly it is dangerous to assign a given precipitate to a particular DSC peak based solely on a comparison with the literature.

The present paper describes an unambiguous TEM identification of the precipitates responsible for DSC peaks observed in a complex casting alloy: 339 aluminum. Also, this study is unique in that it compares two thermal histories of the same alloy: (i) a casting which had been directly-quenched from the die (DQD),

TABLE I Concentrations of primary alloying elements in 339 aluminum castings

	Total Concentration (wt %)			Dendrite Concentration (wt %)		
Sample	Cu	Mg	Si	Cu	Mg	Si
DQD	1.04	0.99	∼12	0.46	0.30	∼1
SOL	1.01	0.78	∼12	0.97	0.48	∼1

to study the sequence of precipitation which would occur during a T5 heat treatment, and (ii) solutionized and quenched material (SOL), to follow the precipitation sequence during a T6 temper.

2. Sample preparation

The DQD samples were cut from a casting which had been quenched in water after removal from the die and then stored in a freezer at −74 °C prior to sample preparation. The SOL samples were cut from an air-cooled casting and subsequently solutionized. During fabrication of samples for the DSC experiments, precautions were taken to minimize exposure to ambient temperatures. DQD samples were removed from the freezer for three brief intervals: (i) initial cutting to rods of square cross section; (ii) machining to cylinders with a diameter of 6 mm; and (iii) slicing discs 2 mm thick. After each step, the samples were returned to the freezer where they remained until just prior to the DSC experiments. Preparation of the SOL samples was simpler because all machining was carried out prior to solution treatment. The samples were solutionized at 510 °C for 3 1/4 hours, quenched in water, then immediately placed in the freezer where they remained until minutes before the DSC experiments.

The two castings had the same nominal composition (12Si/1Mg/1Cu weight percent), but the total Mg content of the SOL sample was about 20% lower than that of the DQD casting (Table I). However, more significant, from the viewpoint of this precipitation study, are the concentrations of solutes retained in the dendrites. These were measured with an electron microprobe and are also listed in Table I.

3. Calorimetry

A Perkin-Elmer DSC7 calorimeter was operated in its temperature-scanned mode to measure the temperature dependence of dQ/dt, the rate of heat absorption or emission by the sample. Such a plot has a baseline proportional to the specific heat of the sample with superimposed endothermic and exothermic peaks due to dissolution and precipitation respectively [31, 32].

Typical DSC thermograms for DQD and SOL 339 aluminum at a heating rate of 20 °C/min are shown in Fig. 1. In each case several exotherms are visible. As discussed above, we can assign the lowest temperature peak(s) to Guinier-Preston (GP) zone formation and the two at higher temperature to precipitation events. The existence of the GP zone peaks indicates that the samples had not been greatly affected by their brief exposure to ambient temperatures during specimen preparation. It is noteworthy that the GP peaks

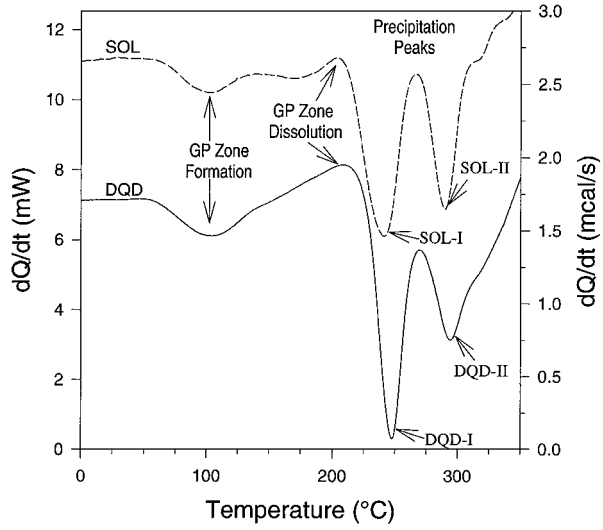

Figure 1 DSC plots of dQ/dt versus temperature for DQD and SOL 339 aluminum at a temperature scan rate of 20 °C/min. The labels indicate the precipitation peaks to which the DSC was scanned to prepare samples for TEM and hardness studies (see text). The two curves are shifted vertically to avoid overlapping.

in the two thermograms differ somewhat in appearance, presumably reflecting the different thermal histories (SOL vs. DQD). These peaks are followed by an endotherm which we attribute to dissolution of the GP zones prior to the exothermic precipitation processes. It is the latter which are examined in detail in the next section.

3. Transmission electron microscopy

Specimens for TEM were prepared in the calorimeter by heating (at 20 °C/min) to either the first or second precipitation peak, after which they were immediately cooled and stored in the freezer. (Zhen *et al.* [29] have used a similar technique.) Four specimens were prepared in this manner: two each for the DQD and SOL castings. The two peaks for the DQD alloy are labeled in Fig. 1 as DQD-I and DQD-II; those for the SOL alloy as SOL-I and SOL-II. These specimens were thinned by mechanical polishing, followed by ion milling. They were then examined in a Philips EM430 scanning transmission electron microscope operating at 300 kV and fitted with a Noran X-ray detector. The precipitates were identified by selected area electron diffraction, and X-ray microanalysis for multiple specimen orientations.

3.1. Precipitates in DQD 339 aluminum

3.1.1. Peak DQD-I

This sample contains primarily thin rod-shaped precipitates about 100 nm long with an aspect ratio larger than 10, oriented along or close to the ⟨100⟩ axes of the Al fcc lattice. When viewed along one of the ⟨100⟩ axes of the matrix, three variants of the precipitates are visible in the micrograph of Fig. 2. The precipitates are coherent with the matrix and have a diffraction pattern (Fig. 2b) characteristic of the ternary S' (Al_2CuMg) phase [40]. Since no other precipitate phase is present in this sample, it is clear that peak DQD-I corresponds to the formation of the S' phase.

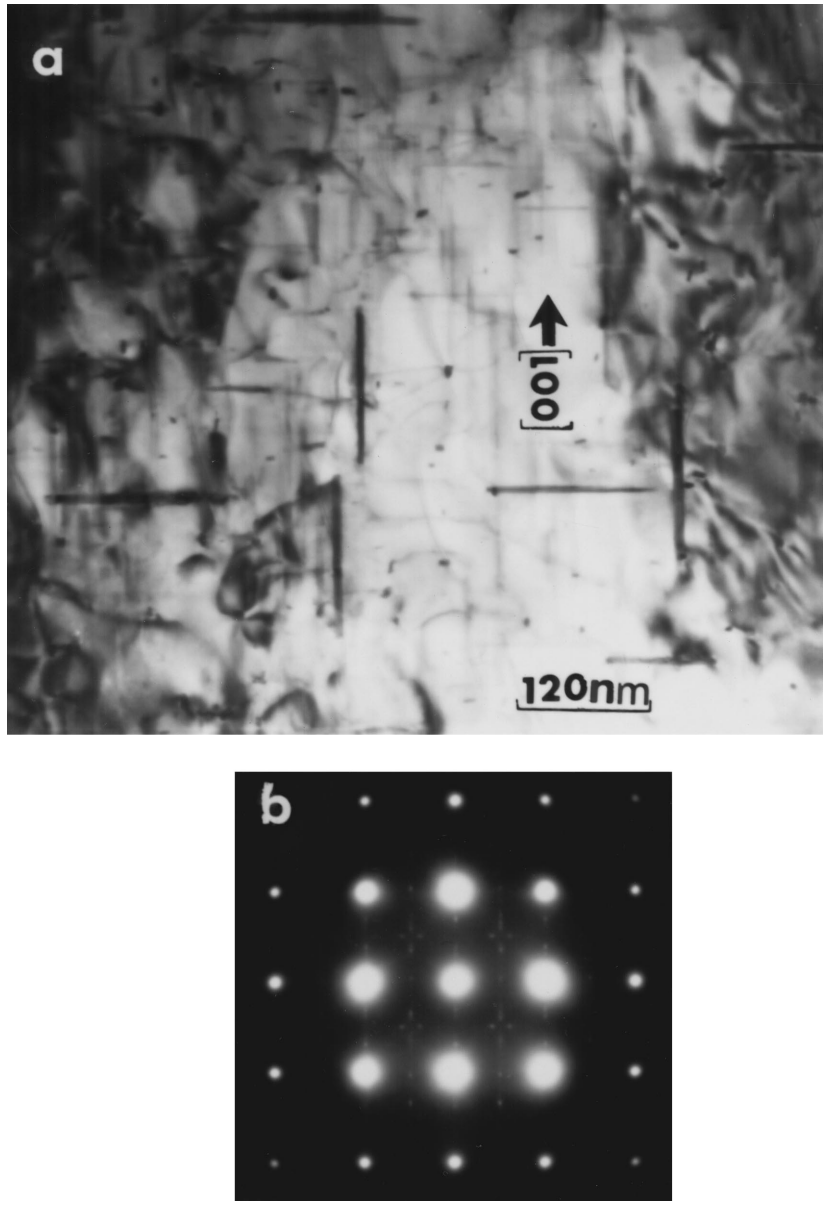

Figure 2 (a) Bright field transmission electron micrograph and (b) corresponding selected area diffraction pattern ([100] zone axis) showing rod shaped S' precipitates in the DQD sample heated to peak DQD-I in Fig. 1 above. The rods parallel to the [100] zone axis appear as dots in the end-on view while the other variants are parallel to the [001] and [010] directions of the Al matrix.

3.1.2. Peak DQD-II

The microstructure of this sample (Fig. 3) contains two different phases: (i) rod-shaped S' phases as discussed above, and (ii) numerous spherical precipitates of Si, as confirmed by selected area diffraction (SAD) and x-ray microanalysis. Thus the second DSC peak is attributed to the precipitation of the Si particles. (Detailed analysis of Si precipitates in 339 Al can be found in reference 41.) The density of the S' precipitates in Fig. 3 is about one third of that found in Fig. 2, indicating that a large fraction of the S' precipitates have re-dissolved as the sample is heated from the DQD-I temperature to the DQD-II temperature. Thus the second DSC peak is attributed to formation of the Si phase.

3.2. Precipitates in solutionized 339 aluminum

3.2.1. Peak SOL-I

The microstructure of this sample (Fig. 4) consists of numerous needle-shaped precipitates dispersed in the fcc Al matrix. These precipitates are ~50 nm long, have an aspect ratio >10, and lie along the [100] axes. The dimensions of the precipitates and their diffraction pattern confirm that the needles are β' (Mg_2Si) precipitates [42] and not β'' or β precipitates. Since no other phase is present in this sample, the SOL-I peak is attributed to the precipitation of the β' phase.

3.2.2. Peak SOL-II

This sample contains only Si precipitates dispersed in the Al matrix [41] (Fig. 5). There is now no evidence of any Mg_2Si phase, indicating that all the Mg_2Si precipitates, which had formed during the temperature scan through Peak SOL-I, have re-dissolved. The size of the Si precipitates ranges from 50 to 60 nm.

4. Dendrite hardness

Some specimens were polished and the hardnesses of the dendrites were measured with a Nanoindenter. A three-sided pyramidal (Berkovitz) diamond was

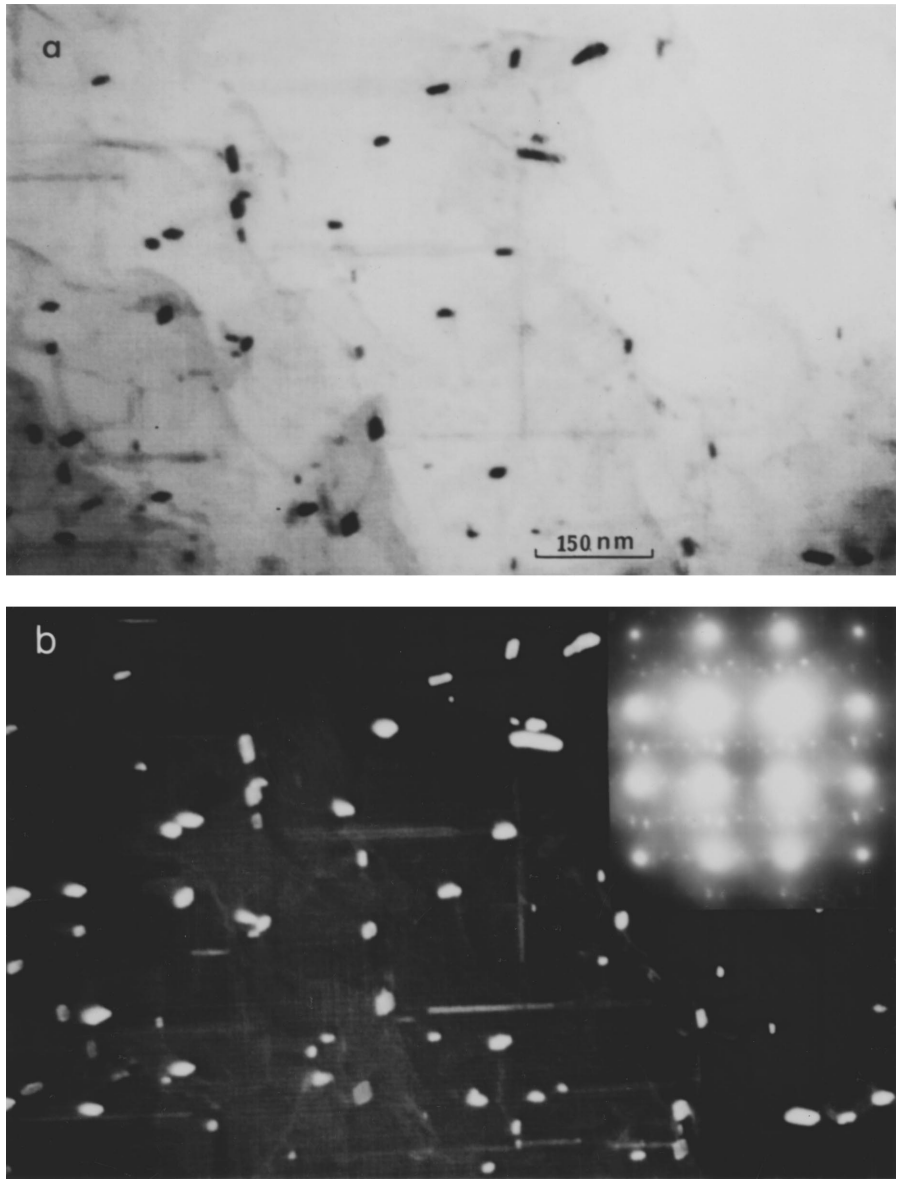

Figure 3 Bright field image for the DQD sample heated to peak DQD-II in Fig. 1. Besides the S' precipitates as in Fig. 2, there are small round Si precipitates dispersed in the sample. The corresponding SAD and dark field images of Si are shown in (b).

applied with a load of 7.5 mN (0.75 g) to ten different dendrites in each specimen. The indentations were typically ∼0.5 μm deep and ∼4 μm wide, positioned in the central region of each dendrite without interference from silicon particles or intermetallics. The thermal histories of these specimens (prior to polishing) are listed in Table II together with their measured dendrite hardnesses. The as-quenched SOL and DQD specimens were measured after 10 hours exposure to room temperature. (This exposure may have resulted in GP-zone formation, but was unlikely to have produced significant precipitation.) Four specimens (two each of SOL and DQD) were heated in the calorimeter to either the first or second precipitation peak, and thus had the same thermal histories as the TEM specimens. In addition, dendrite hardnesses were measured for SOL and DQD specimens scanned in the DSC to 350 °C (as in Fig. 1).

TABLE II Effect of precipitation on dendrite hardness

Thermal History	Hardness (GPa)
As DQD	0.91 ± 0.05
DQD and Heated to Peak DQD-I	1.13 ± 0.09
DQD and Heated to Peak DQD-II	0.95 ± 0.10
DQD and Heated to 350 °C	0.81 ± 0.05
As SOL	0.90 ± 0.05
SOL and Heated to Peak SOL-I	1.24 ± 0.07
SOL and Heated to Peak SOL-II	1.10 ± 0.06
SOL and Heated to 350 °C	0.88 ± 0.02

Initially the SOL and DQD specimens have the same hardness, but after precipitation has occurred, the SOL sample is harder than the DQD. This difference is maintained even after exposure to 350 °C. For both starting conditions, the first precipitation peak corresponds to the highest hardness. Thus, heating to the second peak substantially decreases hardness, which is further reduced after the brief (≤1 min) excursion to 350 °C.

5. Discussion

5.1. The precipitates

The combined DSC/TEM studies have clearly identified the precipitation sequence in 339 aluminum for both the DQD and SOL conditions. In each case

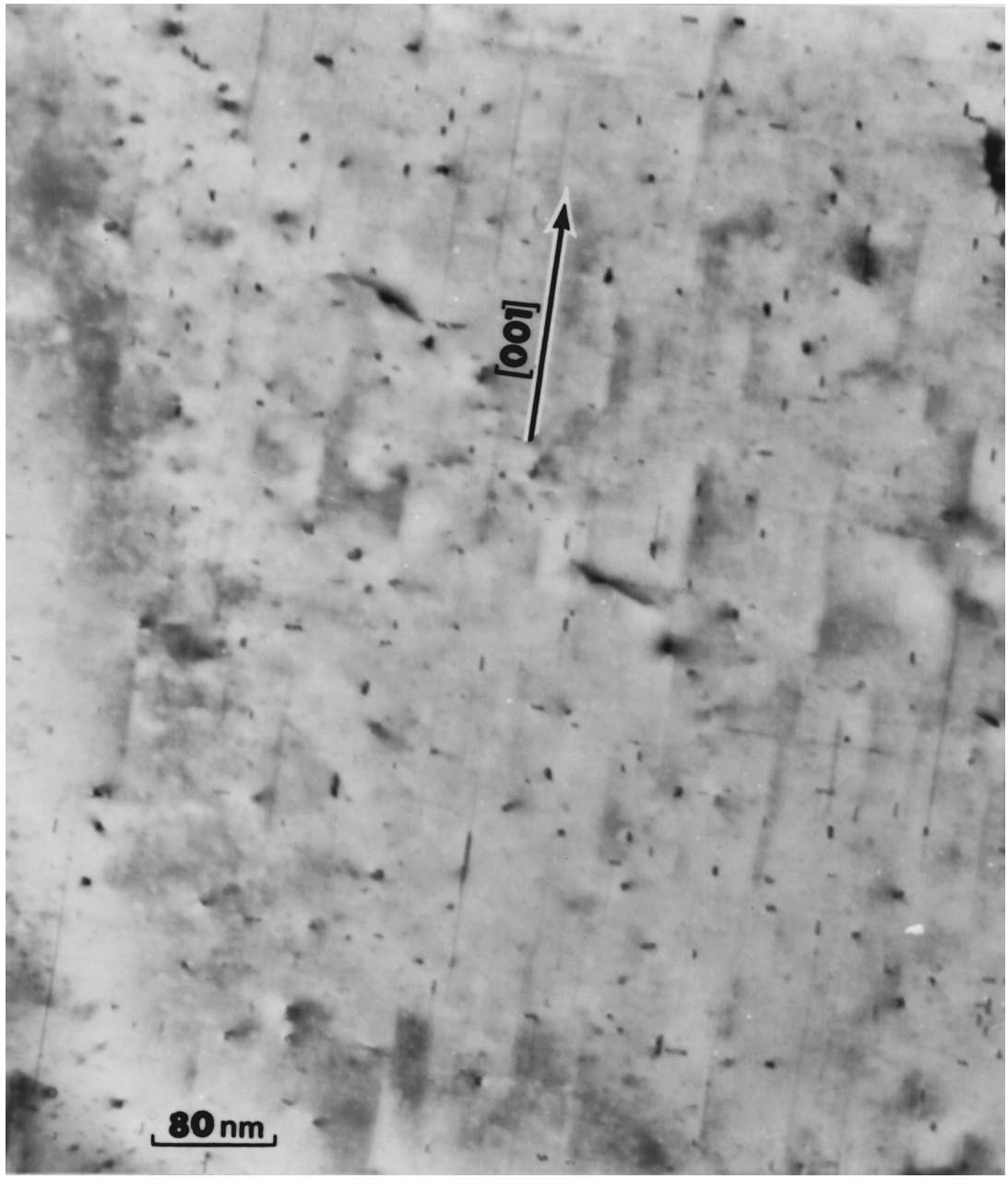

Figure 4 Bright field image of a SOL sample heated to the first DSC peak (SOL-I in Fig. 1) showing small β' precipitates, The dots in the image are β' precipitates viewed end on. The sample has been oriented to weaken the diffraction contrast and dislocations.

there are two pronounced precipitation peaks in the DSC curves; the peak temperatures (at a scan rate of 20 °C/min) and the precipitates are summarized in Table III. In the DQD alloy the lower temperature DSC peak at 247 °C corresponds to the formation of the ternary S' (Al_2CuMg) precipitate. In the solutionized alloy the peak at 240 °C corresponds to the formation of the binary β' precipitate. Apparently the first precipitate to form is controlled by Mg-Cu clusters [43, 44] in the DQD alloy, but by Mg-Si clusters in the SOL alloy. Heating to the second peak dissolves some of the S' phase in the DQD alloy but all of the β' phase in the SOL alloy. At this temperature (290 °C) Si is precipitated in both the SOL and DQD alloys.

TABLE III Precipitation parameters for DQD and SOL 339 aluminum

Peak	Peak T (°C)	Precipitate	$-\Delta Q$ (J/g)
DQD-I	247 ± 1.0	S' (Al_2CuMg)	3.67
DQD-II	295 ± 1.3	Si	3.55
SOL-I	240 ± 2.5	β' (Mg_2Si)	3.52
SOL-II	289 ± 1.0	Si	2.04

Peak temperatures, T, measured at a scan rate of 20 °C/min, are the averages for several samples. $-\Delta Q$ values were derived from 2-gaussian approximations to DSC precipitation peaks (see Figs 4 and 5).

In both the DQD and SOL alloys, the higher hardness is provided by the precipitate formed at the lower temperature peak, namely S' and β' respectively. For the solutionized alloy the reason is very clear from the TEM micrographs: the β' precipitates in Fig. 4 are coherent and more closely spaced than the incoherent Si particles in Fig. 5. Similarly in the case of the DQD alloy, the coherent S' precipitates in Fig. 2 are more effective in blocking dislocation motion than the mixture of S' and incoherent Si precipitates in Fig. 3.

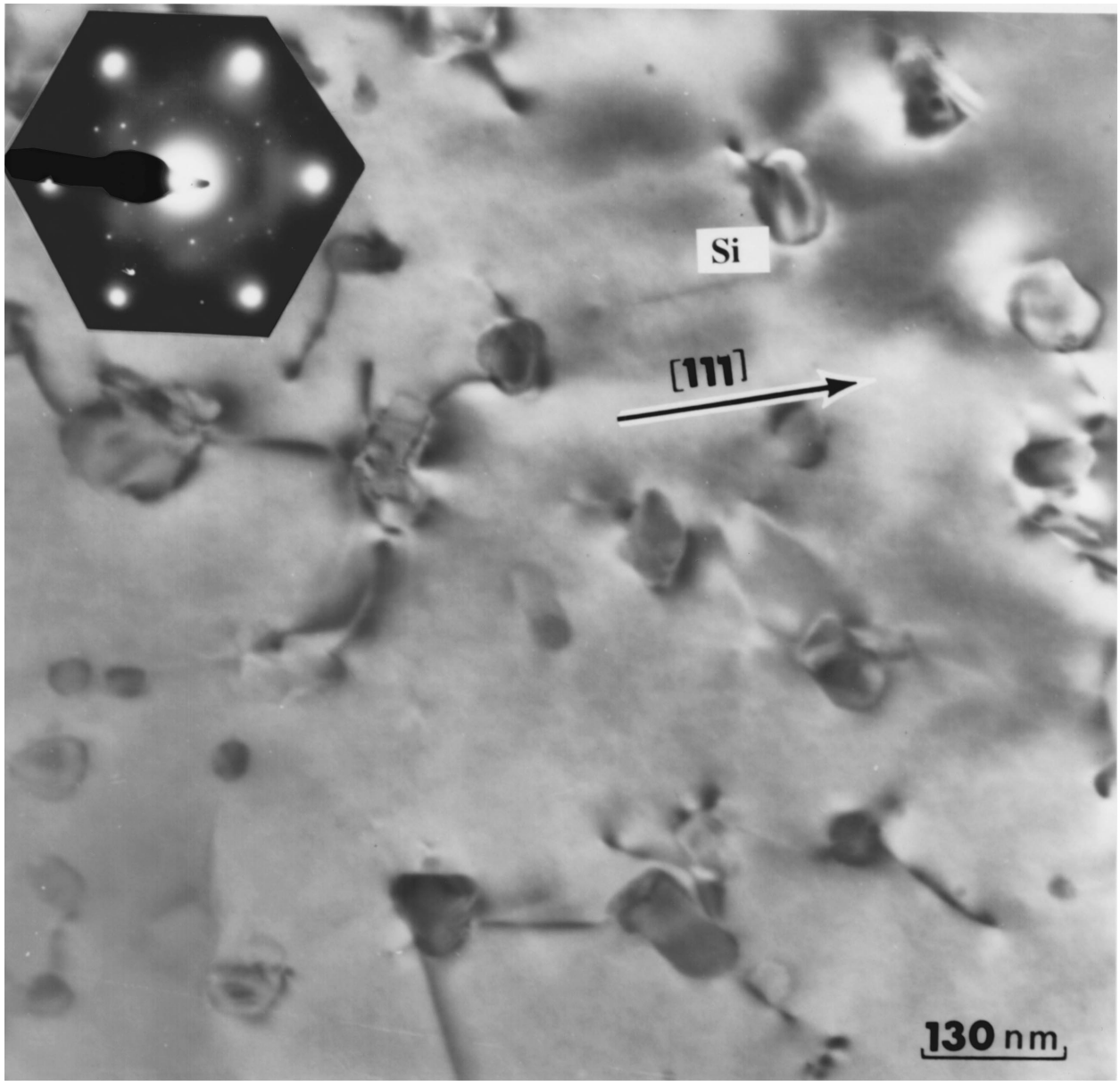

Figure 5 Bright field micrograph and selected area diffraction showing the dispersion of Si particles in the SOL sample heated to the second DSC peak (SOL-II in Fig. 1). There are no other phases present in this sample.

5.2. DSC peaks

The above detailed knowledge of the precipitation processes can only be acquired by the time consuming procedures of TEM, which are not appropriate for routine evaluation of castings. Thus an important question is whether the relatively simple and rapid measurement of the DSC peak structure can provide a unique signature to identify each precipitate and determine its amount. In this regard, the appropriate parameters are the peak temperature and the area of each peak (i.e., the amount of heat released ΔQ). To estimate the latter quantity, the DSC peaks are represented as the sum of two gaussians, as indicated by the dotted curves in Figs 6 and 7. This approximation matches the peaks for the SOL sample (Fig. 7), but it appears that the higher temperature peak of the DQD sample (Fig. 6) overlaps a third smaller peak at ∼340 °C. The ΔQ values derived from the gaussian fits are listed in Table III.

A crucial test is to compare the SOL sample's β' peak at 240 °C with that for S' in the DQD sample at 247 °C. Although the peak temperature difference is

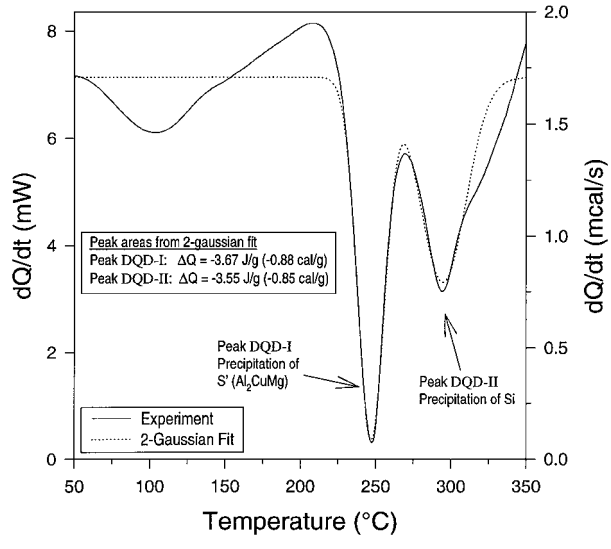

Figure 6 DSC plot of dQ/dt versus temperature for DQD 339 aluminum at a temperature scan rate of 20 °C/min. The dotted curve is the sum of two gaussian curves fitted to the data in order to estimate the amount of heat release associated with each peak (see text).

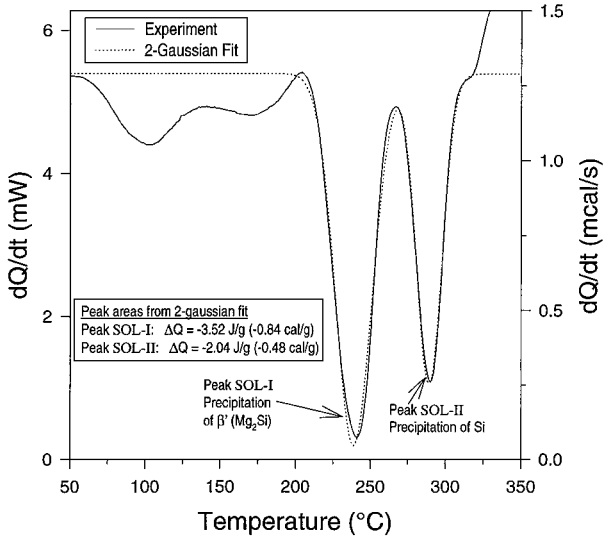

Figure 7 DSC plot of dQ/dt versus temperature for SOL 339 aluminum at a temperature scan rate of 20 °C/min. The dotted curve is a 2-gaussian fit to the data.

only 7 °C, it is still somewhat larger than the specimen-to-specimen variability (Table III). Therefore, we conclude that the formation of the β', S', and Si precipitates in 339 aluminum alloy can be identified on the basis of the peak temperature.

In principle the value of ΔQ for each peak will depend upon the specific precipitate and its concentration, which in turn would be determined by the amount of solute available in the aluminum dendrites and the specific precipitate phase. However, this is not always borne out in practice. For example, the higher temperature Si peak in the SOL specimens substantially smaller than that in the DQD sample despite the fact that the Si particle concentrations are essentially the same (see Figs 3 and 5). This is thought to be due to the fact that in the SOL alloy the β' dissolves completely as Si precipitates, resulting in an endotherm superimposed on the Si precipitation exotherm. The discrepancy is not as sever for the DQD sample, where the S' is more stable and much is retained during Si formation (Fig. 3). Thus we conclude that in this case the value of ΔQ is not an appropriate measure of precipitate density.

6. Conclusions

Based on the results presented here, the following conclusions may be drawn:

1. The sequence of precipitation in 339 aluminum depends upon the thermal history of the alloy.
2. In the solutionized alloy, β' forms first, then dissolves and is replaced by Si.
3. In a casting directly quenched from the die, S' forms first, then partially dissolves as Si forms.
4. The DSC peak temperature identifies the specific precipitate for 339 Al.
5. The peak area (i.e., ΔQ) is not a reliable measure of precipitate density.

Acknowledgements

The authors thank Coleman Jones for providing the 339 Al castings, and Spud Willett, Dick Hall, and Dusanka Radovic for technical assistance.

References

1. K. HIRANO and H. IWASAKI, *Trans. Jap. Inst. Met.* **5** (1964) 162.
2. J. M. PAPAZIAN, *Metall. Trans.* **A12** (1981) 269.
3. M. VAN ROOYAN, J. A. SINTE MAARTENSDIJK and E. J. MITTEMEIJER, *ibid.* **A19** (1988) 2433.
4. C. ANTONIONE, F. MARINO and G. RIONTIONO, *Mater. Chem. Phys.* **20** (1988) 13.
5. S. ABIS and G. DONZELLI, *J. Mater. Sci. Letters* **7** (1988) 51.
6. J. M. PAPAZIAN, *Metall. Trans.* **A19** (1988) 2945.
7. A. K. JENA, A. K. GUPTA and M. C. CHATURVEDI, *Acta. Metall.* **37** (1989) 885.
8. M. C. CHATURVEDI, A. K. GUPTA and A. K. JENA, *Mater. Sci. Eng.* **A110** (1989) 187.
9. M. VAN ROOYAN and E. J. MITTEMEIJER, *Metall. Trans.* **A20** (1989) 1207.
10. I. DUTTA and D. L. BOURELL, *Mater. Sci. Eng.* **A112** (1989) 67.
11. C. BADINI, F. MARINO and A. TOMASI, *Mater. Chem. Phys.* **25** (1990) 57.
12. A.-M. ZAHRA and C. Y. ZAHRA, *J. Thermal Anal.* **36** (1990) 1465.
13. C. BADINI, F. MARINO and A. TOMASI, *Mater. Sci. Eng.* **A136** (1991) 99.
14. *Idem., J. Mater. Sci.* **26** (1991) 6279.
15. P. APPENDINO, C. BADINI, F. MARINO and A. TOMASI, *Mater. Sci. Eng.* **A135** (1991) 275.
16. M. J. STARINK and P. VAN MOURINK, *Metall. Trans* **A20** (1991) 665.
17. M. J. STARINK, V. JOORIS and P. VAN MOURINK, in "Metal Matrix Composites - Processing, Microstructure and Properties," edited by N. Hansen *et al.* (Risϕ National Lab, Roskilde, Denmark, 1991) p. 675.
18. H.-L. LEE, W.-H. LU and S. L.-I. CHAN, *Scripta Metall. Mater.* **25** (1991) 2165.
19. I. DUTTA, S. M. ALLEN and J. L HAFLEY, *Metall. Trans.* **A22** (1991) 2553.
20. I. DUTTA and S. M. ALLEN, *J. Mater. Sci. Letters* **10** (1991) 323.
21. M. J. STARINK and P. VAN MOURINK, *Mater. Sci. Eng.* **A156** (1992) 183.
22. T. S. KIM, T. H. KIM, K. H. OH and H. I. LEE, *J. Mater. Sci.* **27** (1992) 2599.
23. I. DUTTA, C. P. HARPER and G. DUTTA, *Metall. Mater. Trans.* **A25** (1994) 1591.
24. C. GARCIA-CORDOVILLA, E. LOUIS, J. NARCISO and A. PAMIES, *Mater. Sci. Eng.* **A189** (1994) 219.
25. M. P. THOMAS and J. E. KING, *J. Mater. Sci.* **29** (1994) 5272.
26. P. RATCHEV, B. VERLINDEN and P. VANHOUTE, *Scripta Metall. Mater.* **30** (1994) 599.
27. C. BADINI, F. MARINO and E. VERNE, *Mater. Sci. Eng.* **A191** (1995) 185.
28. I. N. A. OGUOCHA and S. YANNACOPOULOS, *ibid.* **A231** (1997) 25.
29. L. ZHEN, W. D. FEI, S. B. KANG and H. W. KIM, *J. Mater. Sci.* **32** (1997) 1895.
30. M. J. STARINK and A.-M. ZAHRA, *Phil. Mag.* **76** (1997) 701.
31. G. W. SMITH, *Thermochimica Acta* **313** (1998) 27.
32. *Idem., ibid.* **317** (1998) 7.
33. H. E. KISSINGER, *Anal. Chem.* **29** (1957) 1702.
34. T. OZAWA, *J. Thermal Anal.* **2** (1970) 301.
35. R. L. THAKUR, in "Advances in Nucleation and Crystallization of Glasses," edited by L. L. Hench and S. W. Freiman (Amer. Ceram. Soc., Columbus, OH, 1972) p. 166.
36. J. A. AUGIS and J. E. BENNETT, *J. Therm. Anal.* **13** (1978) 283.
37. E. J. MITTEMEIJER, L. CHENG, P. J. VAN DER SCHAAF, C. M. BRAKMAN and B. M. KOREVAAR, *Metall. Trans.* **A19** (1988) 925.
38. H. YINNON and D. R. UHLMANN, *J. Non-Crystalline Solids* **54** (1983) 253.
39. J. SESTAK, in "Comprehensive Analytical Chemistry, Vol. XII, Part D," edited by G. Svehla (Elsevier, Amsterdam, 1984) Ch. 9, p. 212.

40. A. K. GUPTA, P. GAUNT and M. C. CHATURVEDI, *Phil. Mag.* **55** (1987) 375.
41. V. RADMILOVIC and R. K. MISHRA, *Scripta Met*, to be published.
42. P. HIRSCH, A. HOWIE, R. B. NICHOLSON, D. W. PASHLEY and M. J. WHELAN, in "Electron Microscopy of Thin Crystals" (Krieger Publishing, Huntington, NY, 1977) p. 151.
43. G. THOMAS and M. J. WHELAN, *Phil. Mag.* **4** (1959) 511.
44. V. RADMILOVIC, G. THOMAS, G. J. SHIFLET and E. A. STARKE, JR., *Scripta Metall* **23** (1989) 1141.

Received 31 August 1999
and accepted 22 February 2000